JCI insight

TRPV4 channels are essential for alveolar epithelial barrier function as protection from lung edema

Jonas Weber, … , Thomas Gudermann, Alexander Dietrich

JCI Insight. 2020. https://doi.org/10.1172/jci.insight.134464.

Research In-Press Preview Cell biology Pulmonology

Graphical abstract

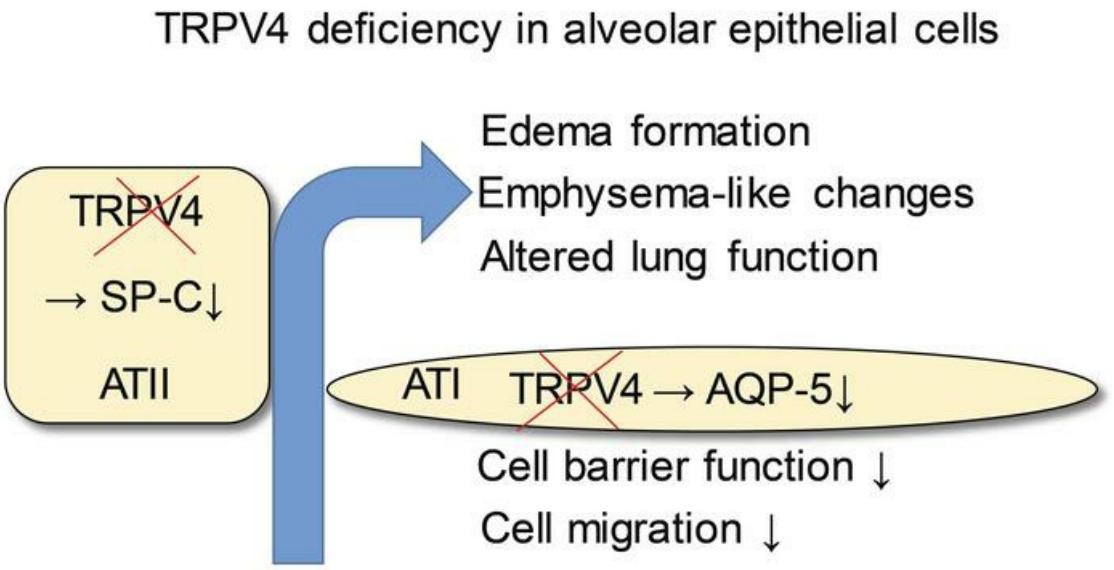

TRPV4 channels are essential for alveolar epithelial barrier function as protection from lung edema

Jonas Weber[1], Suhasini Rajan[1*], Christian Schremmer[1*], Yu-Kai Chao[1], Gabriela Krasteva-Christ[2], Martina Kannler[1], Ali Önder Yildirim[3], Monika Brosien[4], Johann Schredelseker[1], Norbert Weissmann[4], Christian Grimm[1], Thomas Gudermann[1], Alexander Dietrich[1]

[1] Walther Straub Institute of Pharmacology and Toxicology, Member of the German Center for Lung Research (DZL), LMU-Munich, Munich Germany.[2] Institute of Anatomy and Cell Biology, School of Medicine, Saarland University, Homburg, Germany.[3] Comprehensive Pneumology Center (CPC), Institute of Lung Biology and Disease, Member of the German Center for Lung Research (DZL), Helmholtz Center Munich, German Research Center for Environmental Health, Munich, Germany..[4] Justus Liebig University Giessen, Cardio-Pulmonary Institute (CPI), Universities of Giessen and Marburg Lung Center (UGMLC), Giessen, Germany; and member of the German Center for Lung Research (DZL), Germany

*These authors contributed equally to this work

Conflict of interest: The authors have declared that no conflict of interest exists.

Address correspondence to: Alexander Dietrich, Walther-Straub-Institute of Pharmacology and Toxicology, Medical Faculty, LMU-Munich, Nussbaumstr. 26, 800336 Munich, Germany. Phone 011 49 89 2180 73802; Fax 011 49 89 2180 73817, Email: alexander.dietrich@lrz.uni-muenchen.de

Abstract

Ischemia-reperfusion-induced edema (IRE) one of the most significant causes of mortality after lung transplantation can be mimicked ex-vivo in isolated perfused mouse lungs (IPL). Transient receptor potential vanilloid 4 (TRPV4) is a non-selective cation channel studied in endothelium, while its role in the lung epithelium remains elusive. Here we show enhanced IRE in TRPV4-deficient (TRPV4-/-) IPL compared to wild-type (WT) controls, indicating a protective role of TRPV4 to maintain the alveolar epithelial barrier. By immunohistochemistry, mRNA profiling and electrophysiological characterization, we detected TRPV4 in bronchial epithelium, alveolar type I (ATI) and alveolar type II (ATII) cells. Genetic ablation of TRPV4 resulted in reduced expression of the water conducting aquaporin-5 (AQP-5) channel in ATI cells. Migration of TRPV4-/- ATI cells was reduced and cell barrier function was impaired. Analysis of isolated primary TRPV4-deficient ATII cells revealed a reduced expression of surfactant protein C (SP-C) and the TRPV4 activator GSK1016790A induced increases in current densities only in WT ATII cells. Moreover, TRPV4-/- lungs of adult mice developed significantly larger mean chord lengths and altered lung function compared to WT lungs. Therefore, our data discover essential functions of TRPV4 channels in alveolar epithelial cells and in the protection from edema formation.

Introduction

The alveolar epithelium has multiple functions in the lung. On the one hand, the epithelial layer forms a natural barrier to the external environment protecting the body from invading microorganisms and toxicants, while, on the other hand, alveolar epithelial cells facilitate gas exchange. In the adult lung, the alveolar epithelium consists of two epithelial cell types, which are crucial to maintain lung homeostasis and tissue repair (1). Alveolar epithelial type I (ATI) cells are elongated with a large-surface area and high barrier function facilitating gas exchange in close proximity to endothelial cells of the alveolar capillaries (1). ATI cells are also highly water permeable, allowing for ion transport and maintenance of lung fluid balance (2). Although the latter cells cover the largest surface area of the lung (3), alveolar epithelial type II (ATII) cells, which exhibit a cubic morphology, by far outnumber ATI cells (4). ATII cells are also involved in ion transport and liquid homeostasis (5) and are – most importantly - responsible for the production, storage, secretion and recycling of pulmonary surfactant. Surfactant lowers the surface tension at the tissue-air barrier to allow proper inflation and deflation of the alveoli during breathing (6). Moreover, ATII cells also serve as progenitors for ATI cells and are capable of long-term self-renewal (7). Although alveolar epithelial cells express a wide variety of ion transporters and channels (8), the exact roles of these proteins for specialized alveolar cell functions have still remained elusive.

Transient receptor potential vanilloid 4 (TRPV4) is the fourth cloned member of the vanilloid family of TRP channels (9). Like most TRP channels, TRPV4 harbors an invariant sequence, the TRP box (containing the amino acid sequence: EWKFAR), in its intracellular C-terminal tail as well as ankyrin repeats in the intracellular N-terminus.

The protein is composed of six membrane-spanning helices (S1-6), and a presumed pore-forming loop between S5 and S6 (9, 10). Four of these monomers of the same type preferentially assemble in a functional homotetrameric complex (11), although in cilia of renal epithelial cells TRPV4/TRPP2 complexes were also identified (12). Homotetrameric TRPV4 was originally characterized as a sensor of extracellular osmolarity (13, 14). The channel is functionally expressed in endothelial (15, 16) and epithelial cells of the respiratory system (17-19). TRPV4 channels are thermosensitive in the range from 24 to 38 °C and may additionally serve as mechanosensors, because they are activated by membrane and shear stretch as well as by viscous loading (20). As TRPV4 is also involved in pulmonary hypertension (21, 22) and bladder function (23), the channel is an interesting pharmacological target with numerous modulators already identified (reviewed in (24)). Moreover, TRPV4-/- mice were protected from bleomycin-induced pulmonary fibrosis, due to the channel's constitutive expression and function in lung fibroblasts (25). In lung endothelium, where its role was most extensively studied, direct or indirect activation of TRPV4 by mechanical stress (26), high peak inspiratory pressure (27, 28) and high pulmonary venous pressure due to heart failure (29) resulted in the disruption of the endothelial barrier and edema formation. In other tissues however, the channel maintains physiological cell barrier e.g. in skin (30), the urogenital tract (31) and the corneal epithelium (32). In tracheal epithelial cells TRPV4 channels regulate ciliar beat frequency (17) and in alveolar epithelial cells TRPV4 activation by 4α-phorbol esters produced blebs and breaks in lung septa (33) by unknown molecular mechanisms. Moreover, stimulation of TRPV4 by bacterial lipopolysaccharides (LPS) mounted a protective response (34), whereas TRPV4 inhibition reduced lung edema and inflammation after chlorine exposure (35). Therefore, TRPV4 channels may function as chemosensors of toxicants in the lung

epithelium (reviewed in (36)), but their exact role in the alveolar epithelium is still elusive.

We have shown that TRPC6 a member of the classical TRP channel family in the endothelium is increasing endothelial permeability during ischemia/reperfusion (I/R)-induced edema formation (37), one of the most significant causes of mortality after lung transplantation. However, as outlined above, endothelial permeability is also increased by TRPV4 activation (summarized in (38)). Along this line, we analyzed I/R-induced edema formation in a TRPV4-deficient (TRPV4-/-) mouse model. Surprisingly, edema development was increased in TRPV4-/- lungs, but similar to WT in TRPC6/TRPV4 double deficient lungs. These data indicate a protective role for TRPV4 channels in the other natural cell barrier of the lung, the epithelium. Therefore, we set out to study functions of TRPV4 channels in the alveolar epithelium capitalizing on the TRPV4-/- mouse model. Enhanced lung edema formation triggered by ischemia-reperfusion may be probably due to down-regulation of aquaporine-5 channels in ATI cells, reduced surfactant protein-C (SP-C) production in ATII cells and/or emphysema-like changes in the overall lung architecture. Our data suggest an essential role of TRPV4 channels in the alveolar epithelium.

Results

Ablation of TRPV4 increases ischemia-reperfusion (IR)-induced edema formation in isolated perfused mouse lungs. To investigate the role of TRPV4 in IR-induced edema formation, we isolated lungs from wild-type (WT) and TRPV4-deficient (TRPV4-/-) mice. Initial characterization of these mice revealed impaired pressure sensation in dorsal root ganglia (39) and osmotic sensation by exaggerated arginine vasopressin (AVP) secretion in the brain (40). Loss of TRPV4 protein was confirmed in lung lysates. While in WT controls a protein of the appropriate size of 100 kDa was detected by Western- Blotting with TRPV4 specific antibodies, TRPV4-/- lungs did not express any TRPV4 protein (Figure 1A). Murine embryonic fibroblasts (MEF) (41) like pulmonary fibroblasts express TRPV4 protein (25) and served as an additional positive control. After initial perfusion of isolated lungs for 15 min, ischemia was induced for 90 min followed by 120 min reperfusion. TRPV4-/- lungs show enhanced lung edema formation as evidenced by a considerable gain in lung weight as opposed to WT lungs (Figure 1B), whose weight increased to a similar extent as already described by us previously (37). These results clearly contrast with observations on TRPC6-deficient lungs, which are protected from IR-induced edema due to reduced endothelial permeability (37). Therefore, we generated a TRPV4/TRPC6 double deficient mouse model (TRPV4/TRPC6-/-), whose lungs lack the increase in IR-induced edema formation, but developed edema similar to WT mice (Figure 1B). Moreover, lung edema formation in TRPV4-/- lungs was clearly visible by the naked eye (Figure 1C) and consistently wet to dry weight ratio gain doubled in TRPV4-/-, but only slightly increased in TRPV4/TRPC6-/- lungs (Figure 1D). In conclusion, TRPV4 ablation induces increased IR-induced edema, which can be reduced by additional ablation of TRPC6 channels. To identify a possible role for endothelial TRPV4 channels, which

might be activated by shear stress due to hydrostatic pressure (42), we decreased initial flow rates (preflow) from 2ml to 0.5 ml/min. We did not observe any major changes in edema formation in ischemic and non-ischemic WT lungs. TRPV4-/- lungs show a significant decreased edema formation only after 90 and 120 min of reperfusion for unknown reasons (see Supplemental Figure 1).

TRPV4 is expressed in alveolar epithelial type I (ATI) and type II (ATII) cells. As TRPV4 is highly expressed in lung endothelium, and its activation results in an increase of endothelial permeability (reviewed in (38)), we focused on its possible functions in the epithelium. Epithelial cells represent the second natural barrier regulating edema formation. Analysis of mice carrying an enhanced green fluorescent protein (eGFP)-reporter protein under the control of the TRPV4 promoter/enhancer region revealed expression of TRPV4 protein in endothelium, bronchial as well as alveolar epithelium (Figure 2A). In the bronchial epithelium we detected TRPV4 in ciliated cells by co-staining with a β-tubulin IV antibody (Supplemental Figure 2A-C). Neither club nor neuroendocrine cells did show TRPV4 expression (Supplemental Figure 2D-I). In the alveoli, co-staining experiments with an antibody directed against aquaporin-5 (AQP5) (Figure 2B) a marker protein of ATI cells, which are involved in lung septa formation (2), revealed a red staining indicative of AQP-5 expression in the plasma membrane and an additional green staining of the cytosol reflecting TRPV4 expression in these cells (Figure 2B, inset). Moreover, direct quantification of TRPV4 mRNA revealed similar expression levels in ATII cells as in lung endothelial cells (EC), but lower mRNA expression in pulmonary murine lung fibroblasts (pmLF), and precapillary arterial smooth muscle cells (PASMC) (Figure 2C). Therefore, TRPV4 channels are expressed in ATI and ATII cells of the alveolar epithelium.

Loss of TRPV4 resulted in decreased aquaporin-5 expression in ATI cells. Staining of lung slices with fluorescence-coupled antibodies specific for the water conducting channel aquaporin-5 (AQP-5) revealed lower total expression levels in ATI cells and reduced plasma membrane localization in TRPV4-deficient lungs compared to WT lungs (Figure 3A-E). These results were confirmed by Western blotting of lung lysates probed with an AQP-5-specific antibody (Figure 3F-G). In clear contrast to these results, protein levels of aquaporin-1 (AQP-1), a major aquaporin channel in the microvascular endothelium, were not significantly different in TRPV4-/- compared to WT endothelial cells (Supplemental Figure 3A-E). Therefore, AQP5 protein levels in the alveolar epithelium, but not AQP1 expression in the endothelium is reduced by ablation of TRPV4.

Identification of currents induced by the TRPV4 activator GSK1016790A only in primary ATII cells from WT mice. To investigate the role of TRPV4 ~~on~~ at a cellular level, we first isolated ATII epithelial cells (Figure 4A) from WT and TRPV4-deficient mice. We were not able to detect any morphological differences in ATII cells of the different genotypes by phase contrast microscopy. ATII cells were identified by staining with fluorophore-coupled antibodies directed against pro surfactant protein-C (pSP-C) (Figure 4B), which is secreted by ATII cells (reviewed in (5)). Patch clamp analysis of primary ATII cells revealed significantly larger currents, which were induced by the selective TRPV4 activator GSK1016790A (GSK, reviewed in (24)) only in WT cells while currents after the application of GSK1016790A in TRPV4-/- cells were not significantly different to basal currents in WT cells (Figure 4C-D). Western blotting of protein lysates from ATII cells revealed lower pSP-C levels in TRPV4-deficient ATII

cells compared to WT cells (Figure 4E-F). We then differentiated ATII to ATI cells by growing them to confluency in plastic cell culture dishes for at least 6 days as described (1) (Figure 4G). After 6 days WT cells expressed AQP-5 protein as an ATI cell marker (Figure 4H*).* In conclusion, TRPV4 channels are functionally active in ATII cells and are involved in the expression of pSP-C of these alveolar epithelial cells, which can be differentiated to ATI cells *in-vitro*.

TRPV4-/- ATI cells express less AQP-5, show reduced nuclear localization of nuclear factor of activated T-cells (NFAT) as well as decreased cell migration and adhesion. As already shown in lung sections of TRPV4-/- mice translocation of AQP5 to the plasma membrane was reduced in TRPV4-deficient cells (Figure 3A-B). To test if TRPV4-deficient ATII cells are able to differentiate to ATI cells, we analyzed the expression of podoplanin (T1α), another ATI cell marker protein. Notably, podoplanin expression was not significantly different in TRPV4-/- ATII cells differentiated to ATI cells (Figure 4C-D).To further analyze ATI cell function, we quantified nuclear NFATc1 levels. The translocation of NFATc1 protein to the nucleus was significantly reduced in TRPV4-/- cells (Figure 5E-F). Moreover, cell migration analyzed by gap closure in in vitro experiments was clearly slowed down in TRPV4-deficient ATI cells compared to WT cells (Figure 5G-H). As an additional line of evidence we transfected ATII cells with TRPV4-specific or control siRNAs, differentiated them to ATI cells and quantified cell migration in the same way (Supplemental Figure 4). Most interestingly, we obtained similar results as cells transfected with TRPV4-siRNA showed a significantly slower migration compared to non-transfected cells as well as cells transfected with the control siRNAs. As determined by electrical cell impedance sensing (ECIS), sub-confluent TRPV4-/- ATI cells showed reduced cell barrier function (Figure 5I).

Therefore, ablation of TRPV4 induces less AQP-5 expression, reduced nuclear localization of NFAT as well as reduced cell migration and cell barrier function.

TRPV4-/- mice expose emphysema-like lung structures and altered lung function. To analyze differences in lung anatomy as a consequence of altered ATI cell function, we quantified mean chord lengths in histological lung sections (Figure 6A). TRPV4-ablation significantly increased mean chord length of the alveolar lumen in adult (47-52 week old (Figure 6D)) mice compared to WT lungs, while young mice (4-6 weeks old) showed no differences (Figure 6B). Lungs from 28-30 weeks old mice were also prone to larger mean chord lengths (Figure 6C), which however were not significantly different compared to WT lungs. Moreover, lung function was altered (Figure 6E-H): TRPV4-/- lungs showed increased inspiratory capacity and compliance (Figure 6E, G, H) as well as decreased elastance (Figure 6F) significantly different from WT mice of the same age. In conclusion, adult TRPV4-/- mice showed emphysema-like changes in their lungs, which may be responsible for altered lung function.

4. Discussion

Although TRPV4 is highly expressed in lungs, its exact function is still elusive (reviewed in (24)). Activation of TRPV4 in endothelial cells by mechanical stress e.g. stretching (27, 28, 43) as well as oxidative stress by exposure to H_2O_2 (44) resulted in an increased Ca^{2+} influx mediated by the channel and an increase in endothelial permeability conducive to lung edema (reviewed in (38)). Along these lines, pharmacological blockade of TRPV4, e.g. by the specific blocker HC-067047, decreased endothelial rises in intracellular Ca^{2+} and protected mice from vascular leakage and lung injury (28). Expression and function of TRPV4 channels in the alveolar epithelium however, was not studied yet.

Here, we quantified ischemia-reperfusion (IR)-induced edema as one of the most common and significant causes of morbidity and mortality after lung transplantation (45) using the isolated perfused lung model (37). Much to our surprise, TRPV4-/- lungs were not protected from IR-induced lung edema as observed in TRPC6-/- mice (37). On the contrary, genetic TRPV4 ablation resulted in a robust increase in lung edema (Figure 1B) and a higher wet-to-dry weight ratio gain (Figure 1D) when compared to control wild-type (WT) mice. Barrier function was rescued by consecutive breeding TRPV4-/- mice with TRPC6-/- mice, because lung edema formation in double deficient mice was similar to WT animals (Figure 1B).

As TRPV4 activation in endothelial cells has been shown to result in higher edema formation, we focused on the lung epithelium, another physiological cell barrier in the lung. Recent publications indicate an epithelial function of the channel opposed to that in endothelium i.e. stabilization of the epithelial barrier in the skin (30), the urogenital tract (31) and the corneal epithelium (32). We demonstrated TRPV4 expression in alveolar epithelial type I (ATI) and type II (ATII) cells (Figure 2B-C). Our further

molecular analysis corroborated a functional link between TRPV4 and AQP-5, a water conducting channel expressed in ATI cells (46). Hypotonic solutions increased the association and surface localization of TRPV4 and AQP-5 in salivary gland cells (47) and AQP-5 expression is regulated by TRPV4 in lung epithelial cells (48). Most interestingly, the expression and plasma membrane translocation of AQP-5 channels in ATI cells were significantly reduced (Figure 3A-G). Therefore, TRPV4 channels increase AQP-5 expression and translocation in ATI cells in clear contrast to human bronchial epithelial cells where it was reported that activation of TRPV4 channels by shear stress decreased AQP5 levels (47). To analyze TRPV4 function on a cellular level, we isolated ATII cells identified by their expression of pro surfactant protein-C (pSP-C) (Figure 4A-B). We detected significantly larger currents induced by the TRPV4 activator GSK1016790A in WT but not in TRPV4-deficient ATII cells (Figure 4C-D). To our knowledge these data show for the first time that TRPV4 channels are not only expressed, but are also functional in ATII cells. Quantifying pSP-C levels by Western blotting revealed a reduced expression in TRPV4-/- cells compared to WT cells (Figure 4E-F). The role of surfactant proteins in the prevention of alveolar edema by reducing surface tension as a driving force for fluid flow across the air blood barrier, is still a matter of debate (49), but might also explain exaggerated edema formation in TRPV4-/- mice. Therefore, functional TRPV4 and TRPC6 channels are not only located in different cell types like alveolar epithelial and lung endothelial cells, respectively, but may have different roles by decreasing or increasing IR-induced edema. TRPV4 channels aid in epithelial barrier function by supporting SPC production and reducing edema formation in a chronic manner, while TRPC6 channels acutely increase endothelial permeability during IR-induced edema formation (37). Although we cannot exclude a role for endothelial TRPV4 channels, it is unlikely that TRPV4 channels in the endothelium are activated by shear stress due to hydrostatic pressure, as reducing

the preflow in the experiments had no effect on IR-induced edema formation (Supplemental Figure 1).

Next, we differentiated ATII to ATI cells (1), monitored by the expression of two ATI cell markers: AQP-5 and podoplanin. As AQP-5 protein expression was reduced in TRPV4-/- ATI cells (Figure 5A-B), while podoplanin levels were not altered (Figure 5C-D), it seems rather unlikely that TRPV4-deficency and/or a reduction of pSP-C expression results in reduced ATII to ATI differentiation in general. Plasma membrane translocation of AQP-5 as well as AQP-5 expression may depend on nuclear localization of the transcription factor nuclear factor of activated T cells (NFAT) by a rise of intracellular Ca^{2+} via TRPV4 similar to TRPC channels (50). Therefore, we quantified nuclear NFAT levels and detected significantly lower levels in TRPV4-/- cells in comparison to WT control cells (Figure 5E-F). A major breakthrough in our understanding of AQP-5 function for water transport across apical membranes of ATI cells, was the analysis of AQP-5-deficient mice (51). Although lack of AQP-5 entailed a 10-fold decrease in alveolar permeability in response to an osmotic gradient, AQP-5-/- mice are indistinguishable from WT mice with regard to hydrostatic pulmonary edema as well as isoosmolar fluid transport from the alveolar space (51, 52). Cognizant of this scenario, a role for AQP-5 in the clearance of fluid from the alveolar space after IR-induced lung edema cannot entirely be ruled out, but appears to be unlikely, and we tried to dissect other additional mechanisms for the vulnerability of TRPV4-/- lungs to edema formation.

As two reports demonstrated decreased migration of human epithelial ovarian cancer (53) or endometrial adenocarcinoma cells (54) after downregulation of AQP-5, we set out to quantify cell migration of ATII cells differentiated to ATI cells. TRPV4-deficient ATI cells showed a clear deficit in closing gaps by cell migration after releasing inserts

compared to WT cells (Figure 5G-H). In additional experiments, we were able to reproduce these results in cells transfected with TRPV4-siRNAs compared to non-transfected cells as well as cells transfected with control siRNAs (Supplemental Fig. 4). These data suggest an important role of TRPV4 channels in cell migration, which needs to be further analyzed in the future. Moreover, cell resistance as analyzed by electrical cell impedance sensing (ECIS) was significantly reduced in growing TRPV4-/- ATI cells in contrast to WT cells (Figure 5I). Both cell types however reached confluence after 160 h, excluding gross changes in their proliferation rates. Changes in cell morphology were also not detected by microscopy.

ATII cells are able to differentiate to ATI cells after lung injury during repair processes in adult mice (7) to reestablish barrier function of the lung alveolus. Thus, we analyzed lung alveolar histology in WT and TRPV4-/- lungs in young and adult mice. Mean chord length as a measure of alveolar size was increased in adult (47 - 52 weeks old) but not in young (3 weeks old) TRPV4-/- mice compared to WT mice of the same age (Figure 6A-D). We concluded that differences were not caused by defects in embryonic lung development, but were due to ongoing growth and repair processes in adult animals. Most interestingly, the emphysema-like changes in lung morphology were also detected in SP-C-deficient mice (55), raising the possibility that reduced SP-C levels in TRPV4-/- ATII cells may also contribute to the phenotype. In the same vein, adult TRPV4-/- mice showed altered lung function with increased inspiratory capacity and compliance as well as decreased elastance (Figure 6E-H) compared to WT mice of the same age. Loss of septa formation because of reduced SP-C levels in adult TRPV4-/- mice may be responsible for decreased clearance of fluid from the alveolar space and may therefore explain higher edema formation in TRPV4-/- lungs.

In summary, loss of TRPV4 channels in alveolar epithelial cells results in decreased production of pSP-C production in ATII and lower AQP-5 expression and membrane localization in ATI cells. The latter proteins are likely to be involved in continuously ongoing repair processes in adult mice, resulting in emphysema-like changes in TRPV4-/- mice. These chronic events may define a protective function of TRPV4 channels against lung edema formation, in clear contrast to their acute detrimental role in endothelial cells.

Methods

Animals. TRPC6-/- (56), TRPV4-/- (B6.199X1-Trpv4^{tm1MSZ} from Riken BioResource Center (RBRC01939) (39, 40) were backcrossed 10 times to the C57/BL6J strain. TRPC6/TRPV4-/- were obtained by crossing both gene-deficient mouse models. TRPV4eGFP reporter mice (Tg(TRPV4-EGFP)MT43Gsat/ Mmucd from MMRC) were bred as previously described (57). Gender and age matched mice older than 3 months were used in the experiments, if not mentioned otherwise in the figure legends.

Isolated, perfused mouse lung (IPL). Quantification of edema formation in isolated perfused mouse lungs were done as described (37). In brief, mice were anesthetized by intraperitoneal injection of ketamine (100 mg/kg body weight (bw)), xylazine (0,7 mg/kg bw) and anticoagulated with heparin (500 iU./kg bw). Animals were intubated via a small incision in the trachea, ligated and ventilated with room air using the VCM type 681 (positive end−expiratory pressure, 3 cmH_2O; positive end-inspiratory pressure 3 cmH_2O; respiratory rate was 90 breaths/min). The sternum was opened, the ribs were spread and the right ventricle was incised to place the air-free perfusion catheter into the pulmonary artery. After ligation the perfusion was started with 0.5 ml/min perfusion solution (7.19 g sodium chloride, 0.33 g potassium chloride, 0.27 g magnesium hexahydrate, 0.36 g calcium chloride dihydrate, 0.15 g potassium dihydrogen orthophosphate, 2.67 g glucose monohydrate, 51.28 g hydroxyethyl starch 200000/05 ad 1000 ml with aqua ad injectabilia, use 0.1848 mg/ml sodium hydrogen carbonate to adjust pH to 7.3) using an ISAMATEC Tubing Pump. A second perfusion catheter was introduced in the left ventricle and secured by ligation. The lung, together with the trachea and the heart, were excised from the thorax in one piece and transferred to a 37 °C temperature-equilibrated housing chamber of the perfused

mouse lung model (IPL-2, Hugo Sachs Elektronik/Harvard Apparatus (March-Hugstetten, Germany)). The perfusion was slowly raised stepwise to 2 ml/min and perfusion pressure was monitored with the PLUGSYS® TAM-A/P75 type 17111. Weight changes were constantly measured with the edema Balance Module/ EBM type 713. Data was monitored with the Pulmodyn software. The perfusion pressure during the measurements was not significantly different between genotypes as well as before and after ischemia.

Analysis of functional parameters of the respiratory tract. Mice were anesthetized with ketamine (270 mg/kg bw) and xylazin (11 mg/kg bw), intratracheally intubated through a small incision of the trachea and connected to the flexiVent system (Scireq, Montreal, Canada).

Immunohistochemistry. Mouse lungs were inflated with 2.5% (m/v) glutaraldehyde in PBS and processed for paraffin or O.C.T compound (Tissue-Tek, Sakura finetek, Torrance, CA, USA) embedding. Paraffin-embedded tissue sections (3 µm) were cut using a microtome (Zeiss, Göttingen, Germany), mounted on glass slides, deparaffinized in xylene and rehydrated in graded alcohol. Masson Goldner trichrome staining (Masson Goldner Trichrome Staining Kit, Carl Roth 3459) was done according to the manufacturer's instruction with iron hematoxylin solution for 8 min, Goldner's stain 1 for 6 min, Goldner's stain 2 for 1 min and Goldner's stain 3 for 5 min. After dehydration in 100% EtOH and clearing in xylol twice for 1 min, the sections were mounted in Roti-Histokit II (Carl Roth T160.2). Sections were analyzed by design-based stereology using an Olympus BX51 light microscope equipped with the new Computer Assisted Stereological Toolbox (newCAST, Visiopharm) as described (58).

For mean chord length (MCL) measurements, 10-20 frames were selected randomly across multiple sections by the software, using the 20x objective, and superimposed by a line grid and points. The intercepts of lines on alveolar wall (Lsepta) and points localized on air space (Pair) were counted and calculated as MCL (∑Pair × L(p) / ∑Isepta × 0.5, where L(p) is the line length per point). Cryo-embedded lungs were cut in 10 µm sections on a cryostat (Leica, Wetzlar, Germany), mounted on glass slides and surrounded with a hydrophobic pen (Vector Laboratories, California, USA). After washing with PBS the sections were blocked for 30 min in PBS containing 0,2% Triton X-100 and 5% NGS. Incubation with primary antibody was done at 4 °C over-night and secondary antibody at room temperature (RT) for 1 h. Antibodies were diluted in blocking solution. After nuclei staining with Hoechst-dye (2 µg/ml) for 5 min at RT followed by sufficient washing the sections were mounted in Roti-Histokit II. Used antibodies and dilutions were: anti-GFP (chicken, Thermo Fisher, A10262, 1:200), anti-β-tubulin IV (rabbit monoclonal, Abcam, 179509) 1:1600), anti-aquaporin 1 (rabbit, Alomone Labs, AQP-001, 1:100), anti-aquaporin 5 (rabbit, Alomone Labs, AQP-005, 1:100), anti-CC10 (mouse, Santa Cruz, E-11, 1:200) anti-chicken (goat, Thermo Fisher, A11039, 1:400), anti-CGRP (goat, 1:400, Acris, BP022), anti-rabbit IgG (goat, coupled to Alexa 488, Thermo Fisher, A32731, 1:500 and donkey, coupled to Cy3, Merck Millipore, AP182C, 1:1000), anti-goat IgG (donkey, Life Technologies, A11058, 1:400). For direct labeling of the anti-CC10 antibody Zenon Alexa Fluor 546 mouse IgG_1 kit was used according to the manufacturer's recommendations (Invitrogen, 25004). Stained cryosections were analyzed on an epifluorescence microscope (Zeiss Imager.M2, Carl Zeiss, Jena, Germany) and on a confocal microscope (LSM 880, Carl Zeiss). For membrane localization analysis staining intensity was analyzed along a line from the nucleus into the cytosol and the plasma-membrane.

Primary murine alveolar epithelial cells. Isolation of alveolar epithelial cells type 2 (ATII) was done as described (1, 59, 60). In brief, lungs were flushed via a catheter through the pulmonary artery with 0.9% NaCl solution (B. Braun Melsungen AG, Melsungen, Germany), inflated with 1 ml dispase (BD Bioscience, San Jose, CA) followed by 500 µl 1% low-melting-point agarose (Sigma-Aldrich, St Louis, MO) and incubated for 1 h at RT. Subsequently, lung lobes were separated and dissected using two forceps, filtered through 100 µm, 20 µm and 10 µm nylon filters (Sefar, Heiden, Switzerland) and centrifuged for 10 min at 200 x g. Cell pellets were resuspended in DMEM (Sigma-Aldrich) and plated on CD45 and CD16/32 (BD Bioscience) coated culture dishes for a negative selection of macrophages and lymphocytes and incubated for 30 min at 37 °C. Non-adherent cells were collected and seeded on uncoated dishes to negatively select fibroblasts at 37 °C for 25 min. Cells were collected and identified by staining with a fluorescent coupled anti pro surfactant protein C (anti pSP-C antibody, AB3786, Chemicon International, 1:20000). Live cells were counted by trypan blue staining in a Neubauer counting chamber. Two x 10^6 cells/well of a 6-well plate were seeded in DMEM containing 10% FCS (Invitrogen, Carlsbad; USA), 1% HEPES (Carl Roth, Karlsruhe, Germany) and 1% penicillin/streptomycin (Lonza, Basel, Swizerland) and used for analysis or grown for at least 6 d for ATI cell differentiation. ATII cells were transfected with 1 µM Accell SMARTpool siRNA for TRPV4 (in starving medium, 0.1% FCS) two days after isolation. On day 6, the cells were washed once and kept in starving medium. A non-coding pool of the Accell siRNA in starving medium served as control (see Table 2 for siRNA sequences).

Patch Clamp recordings of ATII cells. Conventional whole-cell recordings were carried out at RT 24 h after isolation of ATII cells from WT and TRPV4-deficient mice. The following bath solution containing 140 mM NaCl, 1.3 mM MgCl2, 2.4 mM CaCl2, 10 mM glucose, 10 mM HEPES (pH 7.4 with NaOH) and resulting in an osmolality of 310 mOsm kg-1 was used for patch-clamp recordings. The pipette solution contained 135 mM CsCl, 2 mM Na-ATP, 1 mM $MgCl_2$, 5 mM EGTA and 10 mM HEPES (pH 7.2 with CsOH), resulting in an osmolality of 296 mOsm kg 1. Patch pipettes made of borosilicate glass (Science Products, Hofheim, Germany) had resistances of 2.2-3.5 MΩ for whole-cell measurements. Data were collected with an EPC10 patch clamp amplifier (HEKA, Lambrecht, Germany) using the Patchmaster software. Current density-voltage relations were obtained before and after application of the TRPV4 activator GSK1016790A (1mM) to the bath solution using voltage ramps from –100 to +100 mV, each lasting 5 s. Data were acquired at a frequency of 40 kHz after filtering at 2.8 kHz. The current density-voltage curves and the current density amplitudes at ±100 mV were extracted at minimal or maximal currents, respectively.

Western blot analysis. Western Blotting was done as previously described (61). Chemiluminescence was detected in an Odyssey®Fc unit (Licor, Lincoln, NE, USA). Used antibodies and dilutions were: HRP-conjugated anti-β-actin antibody (Sigma A3854HRP, 1:10000); anti-TRPV4 (rabbit, Abcam ab 39260, 1:1000), anti aquaporin-5 (rabbit, Alomone AQP-005, 1:1000), anti-Podoplanin (goat, R&D Systems AF3244, 1:500), secondary anti-goat IgG (whole molecule)-peroxidase (Sigma A5420-1ML, 1:10000) and secondary anti-rabbit IgG peroxidase (POX)-antibody (Sigma A6154, 1:10000). One representative out of three Western Blots is shown in the figures.

Nanostring® nCounter expression analysis. Direct quantification of TRPV4 mRNA in murine lung cells was done as described (62). In brief: total RNA from pulmonary murine cells was isolated using the Qia RNeasy Mini Kit (Qiagen, Hilden, Germany). Quantity, purity, and integrity of the RNA samples were controlled by spectrophotometry (NanoQuant, Tecan, Männedorf, Switzerland). Two probes (the reporter and the capture probe) were hybridized to their specific target mRNAs. Then, the target-probe complexes were immobilized in the imaging surface of the nCounter Cartridge by binding of the capture probe. Finally, the sample cartridges were scanned by an automated fluorescence microscope and molecular barcodes (fluorophores contained in the reporter probe) for each specific target were counted. For expression analysis by nCounter NanoString technology, 200 ng total RNA was hybridized with a Nanostring Gene Expression CodeSet and analysed using the nCounter Digital Analyzer. Background correction was performed and normalization was applied using 4 different housekeeping genes (Succinate dehydrogenase subunit A (Sdha), β2-microglobuline, glyceraldehyde 3-phosphate dehydrogenase (GAPDH), β-actin). The DNA sequences used for mRNA expression analysis are summarized in Table 1.

Migration assay. Around 4.4 x 10^6 ATII cells/well were seeded on a 2 well silicone insert with a 500 µm cell-free gap (ibidi GmbH, Martinsried, Germany) and grown in DMEM (10% FCS, 1% HEPES and 1% penicillin/streptomycin) for 5 days to obtain ATI like cells. Subsequently cells were starved in serum reduced medium (0.1% FCS) for 24 h before insert detachment to create a defined cell-free gap. Images were taken 0, 1, 3, 5, 8, 12 and 24 h after gap creation. Migration was analyzed by measuring the remaining gap width with ImageJ software in 3 pictures per time point and replicate.

Isolation of nuclear fractions. Isolation of nuclear protein extracts from ATI-like cells after 6 days of culture was performed with a Nuclear Extract Kit according to the manufacturer's instructions (Active Motif, 40010, La Hulpe, Belgium) as described (61). In brief, cells were first washed with PBS containing phosphatase inhibitors. Cytoplasmic protein fractions were collected by adding hypotonic lysis buffer and detergent, causing leakage of cytoplasmic proteins into the supernatant. After centrifugation (14.000 × g for 30 s) nuclear protein fractions were obtained by resuspending pellets in detergent-free lysis buffer containing protease inhibitors. NFAT proteins were analyzed by Western blotting as described below using an NFATc1 specific (mouse, SantaCruz Biotechnology, sc-7294, 1:600) antiserum and lamin B1 (rabbit, Thermo Fisher Scientific, PA5-19468, 1:5000) antibodies as loading control. Protein bands were normalized to loading controls and quantified by an Odyssey® Fc unit (Licor, Lincoln, USA).

Quantification of cell resistance by electrical cell impedance sensing (ECIS). Resistance changes of ATII to ATI cells was analyzed using an electric cell impedance sensing (ECIS) device (Applied Biophysics, Troy, NY, USA). Freshly isolated epithelial cells were seeded on ECIS culture ware (8W10E+; Applied Biophysics, Troy, NY, USA), which was preincubated with FCS for three hours and connected to the ECIS device. A total of 1 x 10^4 cells were seeded per chamber and grown at 37 °C and 5% CO_2 in an incubator. Resistance (Ω) was analyzed at 2000 Hz over 160 hours.

Statistics. All statistical test were performed using GraphPad Prism 7 (GraphPad Software, San Diego, USA). Numbers of mice and cells as well as statistical tests used are indicated in the figure legends. A P-value of <0.05 was considered significant.

Approval of animal experiments. All animal experiments were approved by the local authority (Regierung Oberbayern, Munich, Germany).

Author contributions

JW and AD conceived the study, analyzed data and wrote the manuscript. MB, NW, AÖY, JS, CG aided in the experimental design. JW, Y-KC, CS, MK, GK-C, SR conducted the experiments. TG aided in critical analysis and in revising the article. All authors read the manuscript and provided critical revisions.

Acknowledgements

The authors thank Bettina Braun for excellent technical assistance and the Riken BioResource Center (RBR) as well as the Mutant Mouse Resource and Research Center (MMRRC) for providing the mouse models. This study was funded by the Deutsche Forschungsgemeinschaft (TRR 152, project 16 (AD), project 04 (CG) and project 22 (GKC), GRK 2338, project 04 (AD), project 08 (CG) and the German Center for Lung Research (DZL) (AD; MB, NW, TG).

Figure legends

Table 1. List of oligonucleotides used for nanostring® nCounter expression analysis and siRNAs used for down-regulation of TRPV4 mRNA.

Figure 1. Ablation of TRPV4 increases ischemia-induced edema formation in mouse lungs. (A) TRPV4 protein expression in mouse lungs was evaluated by immunoblotting in whole lung lysates of wild-type (WT) and TRPV4-deficient (TRPV4−/−) mice using a TRPV4-specific antiserum. Murine embryonic fibroblasts (MEF) cells served as additional positive control. Expression of β-actin was used as loading control. (B) Constant weight measurement of ischemic and non-ischemic WT and TRPV4-/- and TRPV4/TRPC6-double deficient (TRPV4/TRPC6-/-) isolated perfused lungs. (C) Representative images of WT and TRPV4-/- lungs after ischemia. (D) Wet-to-dry weight ratio gains of TRPV4-/- and TRPV4/TRPC6-/- lungs compared to WT controls. Data represent means ± SEM of at least 5 lungs for each genotype. Significance between means was analyzed using ANOVA (B, D) and is indicated as *** for $p<0.001$, ** for $p<0.01$ and * for $p<0.05$.

Figure 2. TRPV4 and aquaporin-5 (AQP-5) expression in mouse lungs. (**A**) GFP staining (green) by fluorescent-coupled GFP-specific antibodies in lung cryosections of TRPV4eGFP reporter mice reveals expression of TRPV4 in cells of the lung endothelium (labelled EN) as well as in the bronchial (BE) and alveolar epithelium (AE). Nuclei staining was performed by Hoechst-dye (blue). (**B**) Lung cryosections from TRPV4eGFP- reporter mice were stained with fluorescent-coupled antisera directed against GFP and AQP-5. Confocal images were obtained after excitation at 488 nm (for eGFP, left upper panel marked as green staining) or after excitation at 561 nm (for AQP-5, left lower panel marked as red staining). Both images were merged (right

panel). Nuclei staining was performed by Hoechst-dye (blue). A, alveolus; B, bronchus; V, vasculature. Inset is showing the lower boxed region in a higher magnification (**C**) TRPV4-mRNA quantification in lung cells by the nanostring®-technology. ATII, aleveolar type II cells; EC, endothelial cells; PASMC, precapillary arterial smooth muscle cells; pmLF, primary murine lung fibroblasts. Data represent means ± SEM from at least 3 independent cell isolations.

Figure 3. Aquaporin-5 (AQP-5) expression and translocation to the plasma membrane in WT and TRPV4-/- alveolar epithelial type I (ATI) cells. (**A**) Cryosections of WT and TRPV4-/- lungs stained with an AQP-5 specific fluorescent-coupled antibody. Nuclei staining was performed by Hoechst-dye (blue). Representative histograms for the quantification of AQP-5 protein in the plasma membrane of WT (**B**) and TRPV4-deficient ATI cells (**C**). (**D**, **E**) Summaries of AQP-5 protein expression in plasma membranes (% aquaporine 5 membrane/cytosol (**D**), % AQP-5 in membranes (**E**)). Representative Western blot analysis of AQP-5 expression in WT and TRPV4-/- whole lung lysates (**F**) and summary of AQP-5 expression in lung lysates of TRPV4-/- and WT mice (**G**). Data represent means ± SEM from at least 6 lungs for each genotype. Significance between means was analyzed using two tailed unpaired Student's t-test and indicated as *** for $p<0.001$, ** for $p<0.01$ and * for $p<0.05$.

Figure 4. Identification of alveolar type II (ATII) cells and differentiation to alveolar type I (ATI) cells. (**A**) Representative cell cluster one day after isolation in a phase contrast image and stained with a fluorescent-coupled specific pro surfactant protein-C (pSP-C) antibody (**B**). Nuclei staining was performed by Hoechst-dye (blue).

Electrophysiological whole-cell measurements of basal and GSK1016790A(GSK)-induced current densities in WT and TRPV4-/- primary ATII cells (**C-D**). Representative current density–voltage curves of wild-type (grey, blue traces) and TRPV4-/- (red trace) ATII cells before (grey trace) and during application of GSK1016790A (blue and red traces) (**C**). Summary of current densities at +/-100 mV before (white bars) and after application of GSK1016790A analyzed in WT (black bars) and TRPV4-/- (grey bars) ATII cells (**D**). Representative western blot analysis of pSP-C expression in WT and TRPV4-/- ATII cells (**E**) and summary of pSP-C expression in TRPV4-/- and WT ATII cells (**F**). Image of confluent cells on day 6 after ATII cell isolation (**G**) and analysis of AQP-5 expression in cells grown for 3, 4 and 6 days in plastic cell culture dishes by Western-blotting (**H**). Expression of β-actin was used as loading control in each blot. Data represent means ± SEM from at least 3 independent cell preparations of 5 mice each. Significance between means was analyzed using one way ANOVA (**C**) or two tailed unpaired Student's t-test (**F**) and indicated as ** for $p<0.01$ and * for $p<0.05$.

Figure 5. Nuclear localization of nuclear factor of activated T-cells (NFAT) in and migration and adhesion of TRPV4-deficient and WT ATI cells. Representative western blot analysis of AQP-5 expression in WT and TRPV4-/- ATII cells differentiated to ATI cells (**A**) and summary of AQP-5 expression in these cells (**B**). Representative western blot analysis of podoplanin expression – another ATI cell marker - in WT and TRPV4-/- ATII cells differentiated to ATI cells (**C**) and summary of podoplanin expression in these cells (**D**). Representative western blot analysis of nuclear NFATc1 localization in WT and TRPV4-/- ATI cells (**E**) and summary of nuclear NFAT localization in these cells (**F**). Lamin B1 expression served as loading control. Representative images of a migration assay after removing inserts (**G**). Summary of

remaining gap values normalized to initial values quantified in migration assays of TRPV4-/- and WT ATI cells after releasing inserts at 0, 1, 3, 5, 8, 12 and 24 h (**H**). Electrical cell resistance was quantified with an ECIS device for WT and TRPV4-/- ATI cells for 160 h. (**I**). Data represent means ± SEM from at least 3 independent cell preparations of 5 mice each. Significance between means was analyzed using two tailed unpaired Student's t-test and indicated as *** for $p<0.001$ and * for $p<0.05$.

Figure 6. Chord lengths and lung function of WT and TRPV4-/- mice. Representative images of masson-trichrome-stained lung sections from 52 weeks old WT (left panels) and TRPV4-/- mice (right panels). (**A**). Quantification of mean chord lengths of 4-6 (**B**), 28-30 (**C**) and 47-52 weeks old (**D**) WT and TRPV4-/- mice. Inspiratory capacity (IC (**E**)), elastance of the respiratory system (E_{rs} (**F**)), static compliance (C_{st} (**G**)) and compliance of the respiratory system (C_{rs} (**H**)) of 6 months old WT and TRPV4-/- mice. Data represent means ± SEM from at least 3 mice. Significance between means was analyzed using two tailed unpaired Student's t-test and indicated as *** for $p<0.001$, ** for $p<0.01$ and * for $p<0.05$.

Supplemental Figure 1. Constant weight measurements of ischemic WT and TRPV4-/ isolated perfused lungs after applying preflows (Pre) of different velocities (0.5 ml versus 2ml). Significance between means was analyzed using two way ANOVA and indicated as *** for $p<0.001$ and ** for $p<0.01$.Ablation of TRPV4 increases ischemia-induced edema formation in mouse lungs.

Supplemental Figure 2. Localization of TRPV4 in mouse lungs using immunohistochemistry. *L* = bronchial lumen, *E* = epithelial layer, scale bars = 50 µm. (**A**) Lung cryosections of TRPV4-eGFP reporter mice revealed expression of TRPV4 (arrowheads) in a subpopulation of bronchial epithelial cells. (**B***)*. Ciliated cells were labeled for β-tubulin IV (arrows). (**C**) A merged view of images shown in *A* and *B*. TRPV4eGFP-positive cells are positive for β tubulin IV (double arrowheads, **A-C**). **D-F***)* TRPV4eGFP-fluorescence was enhanced using an anti-GFP-antibody. The same distribution pattern of TRPV4eGFP-immunoreactive cells (arrowheads, **D-F**) was observed. Neuroepithelial bodies labeled by anti-CGRP-antiserum (arrows, E-F) were not immunoreactive for TRPV4eGFP *(merge,* **F***)*. *(***G-I***)* TRPV4eGFP-immunoreactive cells (arrowheads, **G**) were not labeled for CC10 (arrows, **H-I**), a marker for club cells.

Supplemental Figure 3. Aquaporin-1 (AQP-1) expression and translocation to the plasma membrane in WT and TRPV4-/- endothelial cells. Representative histograms for the quantification of AQP-1 protein in the plasma membrane of WT (**A**) and TRPV4-deficient endothelial cells (**B**). Summaries of AQP-1 protein expression in plasma membranes (% AQP-1 in membranes (**C**)) and in relation to the cytosol (% AQP-1 membrane/cytosol (**D**)). Data represent means ± SEM from 9 lungs. No significance between means was identified using two tailed unpaired Student's t-test.

Supplemental Figure 4. Migration of ATI cells expressing TRPV4 siRNA. Summary of remaining gap values normalized to initial values quantified in migration assays of WT ATI cells (control (ctrl) medium) as well as ATI cells transfected with siRNA (non-targeting (nT siRNA) or TRPV4-specific siRNAs (TRPV4 siRNA)) after removing inserts at 0, 1, 3, 5, 8, 12 and 24 h. Data represent means ± SEM from 3

independent cell preparations of 5 mice each. Significance between means was analyzed using two way ANOVA and indicated as *** for $p<0.001$ and * for $p<0.05$.

References

1. Mutze K, Vierkotten S, Milosevic J, Eickelberg O, and Konigshoff M. Enolase 1 (ENO1) and protein disulfide-isomerase associated 3 (PDIA3) regulate Wnt/beta-catenin-driven trans-differentiation of murine alveolar epithelial cells. *Disease models & mechanisms.* 2015;8(8):877-90.
2. Dobbs LG, Johnson MD, Vanderbilt J, Allen L, and Gonzalez R. The great big alveolar TI cell: evolving concepts and paradigms. *Cellular physiology and biochemistry : international journal of experimental cellular physiology, biochemistry, and pharmacology.* 2010;25(1):55-62.
3. Weibel ER. On the tricks alveolar epithelial cells play to make a good lung. *American journal of respiratory and critical care medicine.* 2015;191(5):504-13.
4. Stone KC, Mercer RR, Freeman BA, Chang LY, and Crapo JD. Distribution of lung cell numbers and volumes between alveolar and nonalveolar tissue. *Am Rev Respir Dis.* 1992;146(2):454-6.
5. Fehrenbach H. Alveolar epithelial type II cell: defender of the alveolus revisited. *Respiratory research.* 2001;2(1):33-46.
6. Halliday HL. Surfactants: past, present and future. *J Perinatol.* 2008;28 Suppl 1:S47-56.
7. Desai TJ, Brownfield DG, and Krasnow MA. Alveolar progenitor and stem cells in lung development, renewal and cancer. *Nature.* 2014;507(7491):190-4.
8. Hollenhorst MI, Richter K, and Fronius M. Ion transport by pulmonary epithelia. *J Biomed Biotechnol.* 2011;2011:174306.
9. Nilius B, and Szallasi A. Transient receptor potential channels as drug targets: from the science of basic research to the art of medicine. *Pharmacological reviews.* 2014;66(3):676-814.
10. Dietrich A, Steinritz D, and Gudermann T. Transient receptor potential (TRP) channels as molecular targets in lung toxicology and associated diseases. *Cell Calcium.* 2017;67:123-37.
11. Hellwig N, Albrecht N, Harteneck C, Schultz G, and Schaefer M. Homo- and heteromeric assembly of TRPV channel subunits. *Journal of cell science.* 2005;118(Pt 5):917-28.
12. Kottgen M, Buchholz B, Garcia-Gonzalez MA, Kotsis F, Fu X, Doerken M, et al. TRPP2 and TRPV4 form a polymodal sensory channel complex. *J Cell Biol.* 2008;182(3):437-47.
13. Liedtke W, Choe Y, Marti-Renom MA, Bell AM, Denis CS, Sali A, et al. Vanilloid receptor-related osmotically activated channel (VR-OAC), a candidate vertebrate osmoreceptor. *Cell.* 2000;103(3):525-35.
14. Strotmann R, Harteneck C, Nunnenmacher K, Schultz G, and Plant TD. OTRPC4, a nonselective cation channel that confers sensitivity to extracellular osmolarity. *Nat Cell Biol.* 2000;2(10):695-702.
15. Hill-Eubanks DC, Gonzales AL, Sonkusare SK, and Nelson MT. Vascular TRP channels: performing under pressure and going with the flow. *Physiology (Bethesda).* 2014;29(5):343-60.
16. Marziano C, Hong K, Cope EL, Kotlikoff MI, Isakson BE, and Sonkusare SK. Nitric Oxide-Dependent Feedback Loop Regulates Transient Receptor Potential Vanilloid 4 (TRPV4) Channel Cooperativity and Endothelial Function in Small Pulmonary Arteries. *J Am Heart Assoc.* 2017;6(12).
17. Lorenzo IM, Liedtke W, Sanderson MJ, and Valverde MA. TRPV4 channel participates in receptor-operated calcium entry and ciliary beat frequency regulation in mouse airway epithelial cells. *Proc Natl Acad Sci U S A.* 2008;105(34):12611-6.
18. Li J, Kanju P, Patterson M, Chew WL, Cho SH, Gilmour I, et al. TRPV4-mediated calcium influx into human bronchial epithelia upon exposure to diesel exhaust particles. *Environ Health Perspect.* 2011;119(6):784-93.
19. Henry CO, Dalloneau E, Perez-Berezo MT, Plata C, Wu Y, Guillon A, et al. In vitro and in vivo evidence for an inflammatory role of the calcium channel TRPV4 in lung epithelium: Potential involvement in cystic fibrosis. *American journal of physiology Lung cellular and molecular physiology.* 2016;311(3):L664-75.

20. Goldenberg NM, Ravindran K, and Kuebler WM. TRPV4: physiological role and therapeutic potential in respiratory diseases. *Naunyn Schmiedebergs Arch Pharmacol.* 2015;388(4):421-36.
21. Xia Y, Fu Z, Hu J, Huang C, Paudel O, Cai S, et al. TRPV4 channel contributes to serotonin-induced pulmonary vasoconstriction and the enhanced vascular reactivity in chronic hypoxic pulmonary hypertension. *Am J Physiol Cell Physiol.* 2013;305(7):C704-15.
22. Goldenberg NM, Wang L, Ranke H, Liedtke W, Tabuchi A, and Kuebler WM. TRPV4 Is Required for Hypoxic Pulmonary Vasoconstriction. *Anesthesiology.* 2015;122(6):1338-48.
23. Everaerts W, Zhen X, Ghosh D, Vriens J, Gevaert T, Gilbert JP, et al. Inhibition of the cation channel TRPV4 improves bladder function in mice and rats with cyclophosphamide-induced cystitis. *Proc Natl Acad Sci U S A.* 2010;107(44):19084-9.
24. Dietrich A. Modulators of Transient Receptor Potential (TRP) Channels as Therapeutic Options in Lung Disease. *Pharmaceuticals (Basel).* 2019;12(1).
25. Rahaman SO, Grove LM, Paruchuri S, Southern BD, Abraham S, Niese KA, et al. TRPV4 mediates myofibroblast differentiation and pulmonary fibrosis in mice. *J Clin Invest.* 2014;124(12):5225-38.
26. Jian MY, King JA, Al-Mehdi AB, Liedtke W, and Townsley MI. High vascular pressure-induced lung injury requires P450 epoxygenase-dependent activation of TRPV4. *American journal of respiratory cell and molecular biology.* 2008;38(4):386-92.
27. Hamanaka K, Jian MY, Weber DS, Alvarez DF, Townsley MI, Al-Mehdi AB, et al. TRPV4 initiates the acute calcium-dependent permeability increase during ventilator-induced lung injury in isolated mouse lungs. *American journal of physiology Lung cellular and molecular physiology.* 2007;293(4):L923-32.
28. Michalick L, Erfinanda L, Weichelt U, van der Giet M, Liedtke W, and Kuebler WM. Transient Receptor Potential Vanilloid 4 and Serum Glucocorticoid-regulated Kinase 1 Are Critical Mediators of Lung Injury in Overventilated Mice In Vivo. *Anesthesiology.* 2017;126(2):300-11.
29. Thorneloe KS, Cheung M, Bao W, Alsaid H, Lenhard S, Jian MY, et al. An orally active TRPV4 channel blocker prevents and resolves pulmonary edema induced by heart failure. *Science translational medicine.* 2012;4(159):159ra48.
30. Akazawa Y, Yuki T, Yoshida H, Sugiyama Y, and Inoue S. Activation of TRPV4 strengthens the tight-junction barrier in human epidermal keratinocytes. *Skin Pharmacol Physiol.* 2013;26(1):15-21.
31. Janssen DA, Jansen CJ, Hafmans TG, Verhaegh GW, Hoenderop JG, Heesakkers JP, et al. TRPV4 channels in the human urogenital tract play a role in cell junction formation and epithelial barrier. *Acta Physiol (Oxf).* 2016;218(1):38-48.
32. Martinez-Rendon J, Sanchez-Guzman E, Rueda A, Gonzalez J, Gulias-Canizo R, Aquino-Jarquin G, et al. TRPV4 Regulates Tight Junctions and Affects Differentiation in a Cell Culture Model of the Corneal Epithelium. *J Cell Physiol.* 2017;232(7):1794-807.
33. Alvarez DF, King JA, Weber D, Addison E, Liedtke W, and Townsley MI. Transient receptor potential vanilloid 4-mediated disruption of the alveolar septal barrier: a novel mechanism of acute lung injury. *Circ Res.* 2006;99(9):988-95.
34. Alpizar YA, Boonen B, Sanchez A, Jung C, Lopez-Requena A, Naert R, et al. TRPV4 activation triggers protective responses to bacterial lipopolysaccharides in airway epithelial cells. *Nature communications.* 2017;8(1):1059.
35. Balakrishna S, Song W, Achanta S, Doran SF, Liu B, Kaelberer MM, et al. TRPV4 inhibition counteracts edema and inflammation and improves pulmonary function and oxygen saturation in chemically induced acute lung injury. *American journal of physiology Lung cellular and molecular physiology.* 2014;307(2):L158-72.
36. Steinritz D, Stenger B, Dietrich A, Gudermann T, and Popp T. TRPs in Tox: Involvement of Transient Receptor Potential-Channels in Chemical-Induced Organ Toxicity-A Structured Review. *Cells.* 2018;7(8).

37. Weissmann N, Sydykov A, Kalwa H, Storch U, Fuchs B, Mederos y Schnitzler M, et al. Activation of TRPC6 channels is essential for lung ischaemia-reperfusion induced oedema in mice. *Nature communications.* 2012;3:649.
38. Simmons S, Erfinanda L, Bartz C, and Kuebler WM. Novel mechanisms regulating endothelial barrier function in the pulmonary microcirculation. *J Physiol.* 2018.
39. Suzuki M, Mizuno A, Kodaira K, and Imai M. Impaired pressure sensation in mice lacking TRPV4. *J Biol Chem.* 2003;278(25):22664-8.
40. Mizuno A, Matsumoto N, Imai M, and Suzuki M. Impaired osmotic sensation in mice lacking TRPV4. *Am J Physiol Cell Physiol.* 2003;285(1):C96-101.
41. Kalwa H, Storch U, Demleitner J, Fiedler S, Mayer T, Kannler M, et al. Phospholipase C epsilon (PLCepsilon) induced TRPC6 activation: a common but redundant mechanism in primary podocytes. *J Cell Physiol.* 2015;230(6):1389-99.
42. Mendoza SA, Fang J, Gutterman DD, Wilcox DA, Bubolz AH, Li R, et al. TRPV4-mediated endothelial Ca2+ influx and vasodilation in response to shear stress. *Am J Physiol Heart Circ Physiol.* 2010;298(2):H466-76.
43. Yin J, Hoffmann J, Kaestle SM, Neye N, Wang L, Baeurle J, et al. Negative-feedback loop attenuates hydrostatic lung edema via a cGMP-dependent regulation of transient receptor potential vanilloid 4. *Circ Res.* 2008;102(8):966-74.
44. Suresh K, Servinsky L, Reyes J, Baksh S, Undem C, Caterina M, et al. Hydrogen peroxide-induced calcium influx in lung microvascular endothelial cells involves TRPV4. *American journal of physiology Lung cellular and molecular physiology.* 2015;309(12):L1467-77.
45. de Perrot M, Liu M, Waddell TK, and Keshavjee S. Ischemia-reperfusion-induced lung injury. *American journal of respiratory and critical care medicine.* 2003;167(4):490-511.
46. Dobbs LG, Gonzalez R, Matthay MA, Carter EP, Allen L, and Verkman AS. Highly water-permeable type I alveolar epithelial cells confer high water permeability between the airspace and vasculature in rat lung. *Proc Natl Acad Sci U S A.* 1998;95(6):2991-6.
47. Liu X, Bandyopadhyay BC, Nakamoto T, Singh B, Liedtke W, Melvin JE, et al. A role for AQP5 in activation of TRPV4 by hypotonicity: concerted involvement of AQP5 and TRPV4 in regulation of cell volume recovery. *J Biol Chem.* 2006;281(22):15485-95.
48. Sidhaye VK, Guler AD, Schweitzer KS, D'Alessio F, Caterina MJ, and King LS. Transient receptor potential vanilloid 4 regulates aquaporin-5 abundance under hypotonic conditions. *Proc Natl Acad Sci U S A.* 2006;103(12):4747-52.
49. Hills BA. An alternative view of the role(s) of surfactant and the alveolar model. *J Appl Physiol (1985).* 1999;87(5):1567-83.
50. Curcic S, Schober R, Schindl R, and Groschner K. TRPC-mediated Ca(2+) signaling and control of cellular functions. *Semin Cell Dev Biol.* 2019.
51. Ma T, Fukuda N, Song Y, Matthay MA, and Verkman AS. Lung fluid transport in aquaporin-5 knockout mice. *J Clin Invest.* 2000;105(1):93-100.
52. King LS, Nielsen S, and Agre P. Aquaporins and the respiratory system: advice for a lung investigator. *J Clin Invest.* 2000;105(1):15-6.
53. Yan C, Zhu Y, Zhang X, Chen X, Zheng W, and Yang J. Down-regulated aquaporin 5 inhibits proliferation and migration of human epithelial ovarian cancer 3AO cells. *J Ovarian Res.* 2014;7:78.
54. Jiang XX, Xu KH, Ma JY, Tian YH, Guo XY, Lin J, et al. Reduced migration of Ishikawa cells associated with downregulation of aquaporin-5. *Oncol Lett.* 2012;4(2):257-61.
55. Glasser SW, Detmer EA, Ikegami M, Na CL, Stahlman MT, and Whitsett JA. Pneumonitis and emphysema in sp-C gene targeted mice. *J Biol Chem.* 2003;278(16):14291-8.
56. Dietrich A, Mederos YSM, Gollasch M, Gross V, Storch U, Dubrovska G, et al. Increased vascular smooth muscle contractility in TRPC6-/- mice. *Mol Cell Biol.* 2005;25(16):6980-9.
57. Gong S, Zheng C, Doughty ML, Losos K, Didkovsky N, Schambra UB, et al. A gene expression atlas of the central nervous system based on bacterial artificial chromosomes. *Nature.* 2003;425(6961):917-25.

58. John-Schuster G, Hager K, Conlon TM, Irmler M, Beckers J, Eickelberg O, et al. Cigarette smoke-induced iBALT mediates macrophage activation in a B cell-dependent manner in COPD. *American journal of physiology Lung cellular and molecular physiology.* 2014;307(9):L692-706.
59. Corti M, Brody AR, and Harrison JH. Isolation and primary culture of murine alveolar type II cells. *American journal of respiratory cell and molecular biology.* 1996;14(4):309-15.
60. Dobbs LG. Isolation and culture of alveolar type II cells. *The American journal of physiology.* 1990;258(4 Pt 1):L134-47.
61. Hofmann K, Fiedler S, Vierkotten S, Weber J, Klee S, Jia J, et al. Classical transient receptor potential 6 (TRPC6) channels support myofibroblast differentiation and development of experimental pulmonary fibrosis. *Biochim Biophys Acta.* 2017;1863(2):560-8.
62. Kannler M, Luling R, Yildirim AO, Gudermann T, Steinritz D, and Dietrich A. TRPA1 channels: expression in non-neuronal murine lung tissues and dispensability for hyperoxia-induced alveolar epithelial hyperplasia. *Pflugers Arch.* 2018.

Table 1. List of oligonucleotides used for nanostring® nCounter expression analysis

Primer pool A

Name	Primer sequence	Gene Id.
β-Actin	AAAAGAGCCTCAGGGCATCGGAACCGCT CGTTGCCAATAGTGATGACCTGCCTCAAG ACCTAAGCGACAGCGTGACCTTGTTTCA	NM_007393.1:815
β2-Microglobulin	ATTTGGATTTCAATGTGAGGCGGGTGGA ACTGTGTTACGTAGCAGTTCAGCATCCTCT TCTTTTCTTGGTGTTGAGAAGATGCTC	NM_009735.3:177
Succinate dehydrogenase subunit A (SdHa)	GGCATGCAGTATTAAACCCTGCCTCAGAA AGGCCAAATGCAGCTCGCAAGCACAATTC TGCGGGTTAGCAGGAAGGTTAGGGAAC	NM_023281.1:250
GAPDH	ATCGAAGGTGGAAGAGTGGGAGTTGCTG TTGAAGTCGCAGGAGACAACCTCTGTTGA GATTATTGAGCTTCATCATGACCAGAAG	NM_001001303.1:890
TRPV4	GGCCTCGGTAGTAGATGTCTCTGAAGGG CGAGTTGATGAATTCACGCATGCATAAAA TTGGTTTTGCCTTTCAGCAATTCAACTT	NM_022017.3:776

Primer pool B

Name	Primer sequence	Gene Id.
β-Actin	CGAAAGCCATGACCTCCGATCACTCATGT AGTTTCATGGATGCCACAGGATTCCATAC CCAAGAAGGAAGGCTGG	NM_007393.1:815
β2-Microglobulin	CGAAAGCCATGACCTCCGATCACTCAGGA CATATCTGACATCTCTACTTTAGGAATTTT TTTCCCGTTCTTCAGC	NM_009735.3:177
Succinate dehydrogenase subunit A (SdHa)	CGAAAGCCATGACCTCCGATCACTCCTCC CTGTGCTGCAACAGTATGTGATCGGGTAG GAAAGAGCTTTGTAA	NM_023281.1:250
GAPDH	CGAAAGCCATGACCTCCGATCACTCCAGG AAATGAGCTTGACAAAGTTGTCATTGAGA GCAATGCCAGCCCCGGC	NM_001001303.1:890
TRPV4	CGAAAGCCATGACCTCCGATCACTCCACG TAGTGCTTGCAGCGCCGTTCGATGGCAAT GTGCAGGGATGTCT	NM_022017.3:776

Table 2. List of siRNAs used for down-regulation of TRPV4 mRNA.

Accell Mouse TRPV4 siRNA- SMARTpool

Name	Target Sequence
Accell SMARTpool siRNA A-040742-13	CCAUUGACCUGUUGGAGUC
Accell SMARTpool siRNA A-040742-14	GCAACAUGCGUGAAUUCAU
Accell SMARTpool siRNA A-040742-15	UUACCAGUAUCAAAGACUU
Accell SMARTpool siRNA A-040742-16	CUCUUGUGUAUUAUUUAUU

Accell Non-targeting Pool

Name	Target Sequence
Accell Non-targeting Pool D-001910-10-20	UGGUUUACAUGUCGACUAA
	UGGUUUACAUGUUUUCUGA
	UGGUUUACAUGUUUUCCUA
	UGGUUUACAUGUUGUGUGA

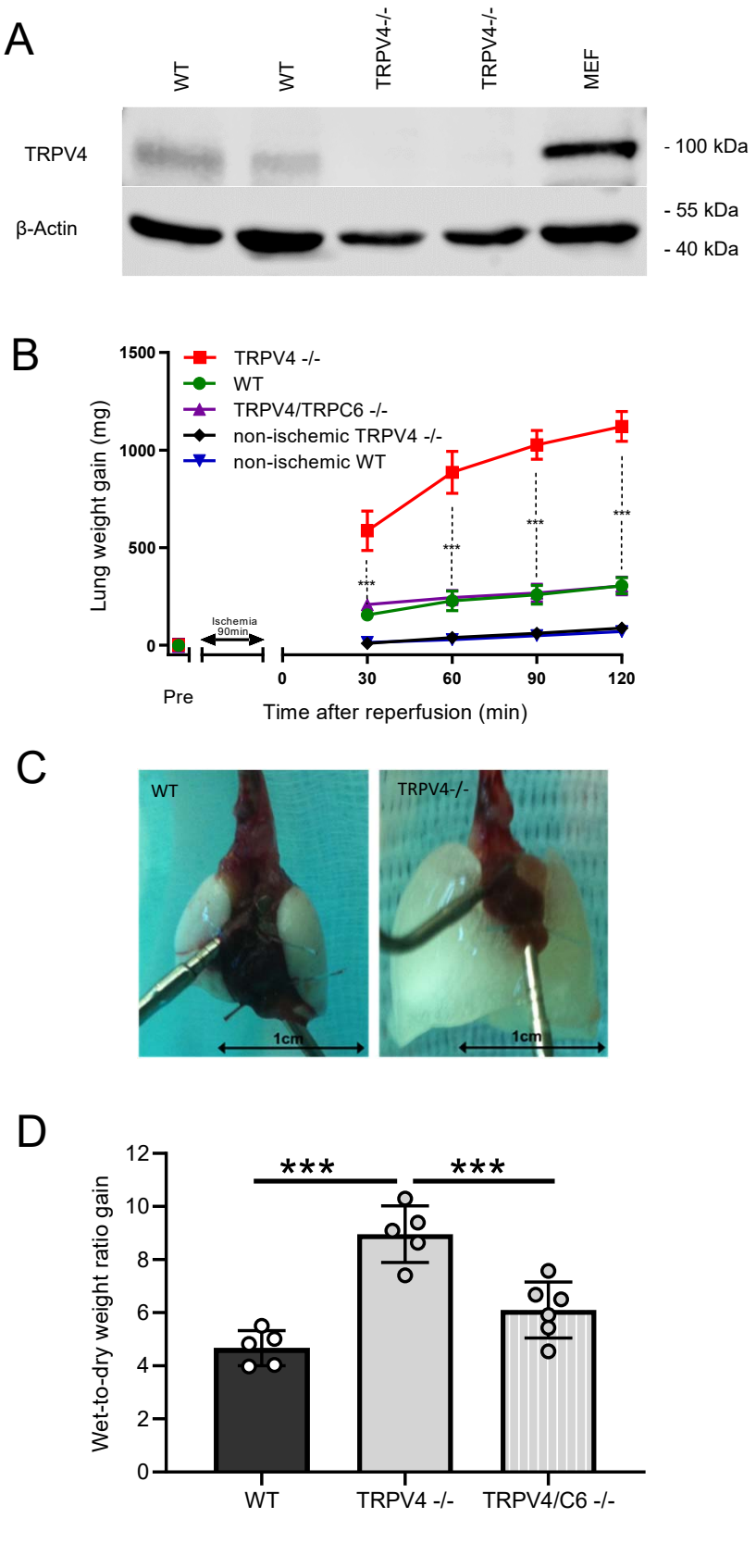
A
WT
WT
TRPV4-/-
TRPV4-/-
MEF
TRPV4
β-Actin
- 100 kDa
- 55 kDa
- 40 kDa
B
TRPV4 -/-
WT
TRPV4/TRPC6 -/-
non-ischemic TRPV4 -/-
non-ischemic WT
Lung weight gain (mg)
1500
1000
500
0
Ischemia
90min
Pre
0
30
60
90
120
Time after reperfusion (min)
***
C
WT
TRPV4-/-
1cm
1cm
D
Wet-to-dry weight ratio gain
12
10
8
6
4
2
0
***
***
WT
TRPV4 -/-
TRPV4/C6 -/-

Figure 1

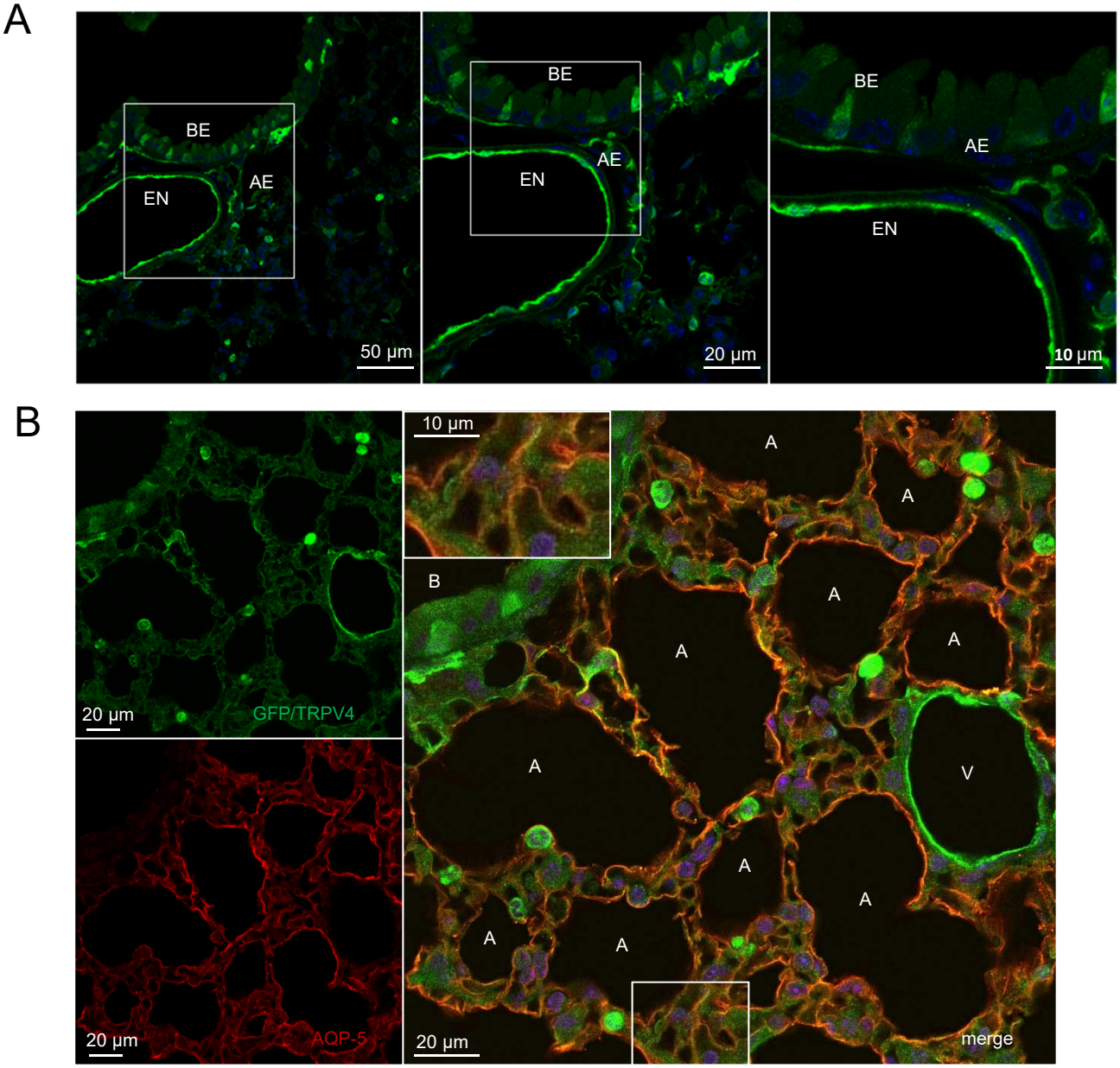
A
BE
AE
EN
50 µm
BE
AE
EN
20 µm
BE
AE
EN
10 µm
B
10 µm
20 µm
GFP/TRPV4
20 µm
AQP-5
B
A
V
20 µm
merge
C
Normalized counts in 200ng RNA - neg. controls
500
400
300
200
100
0
-100
pmLF
PASMC
ATII
EC

Figure 2

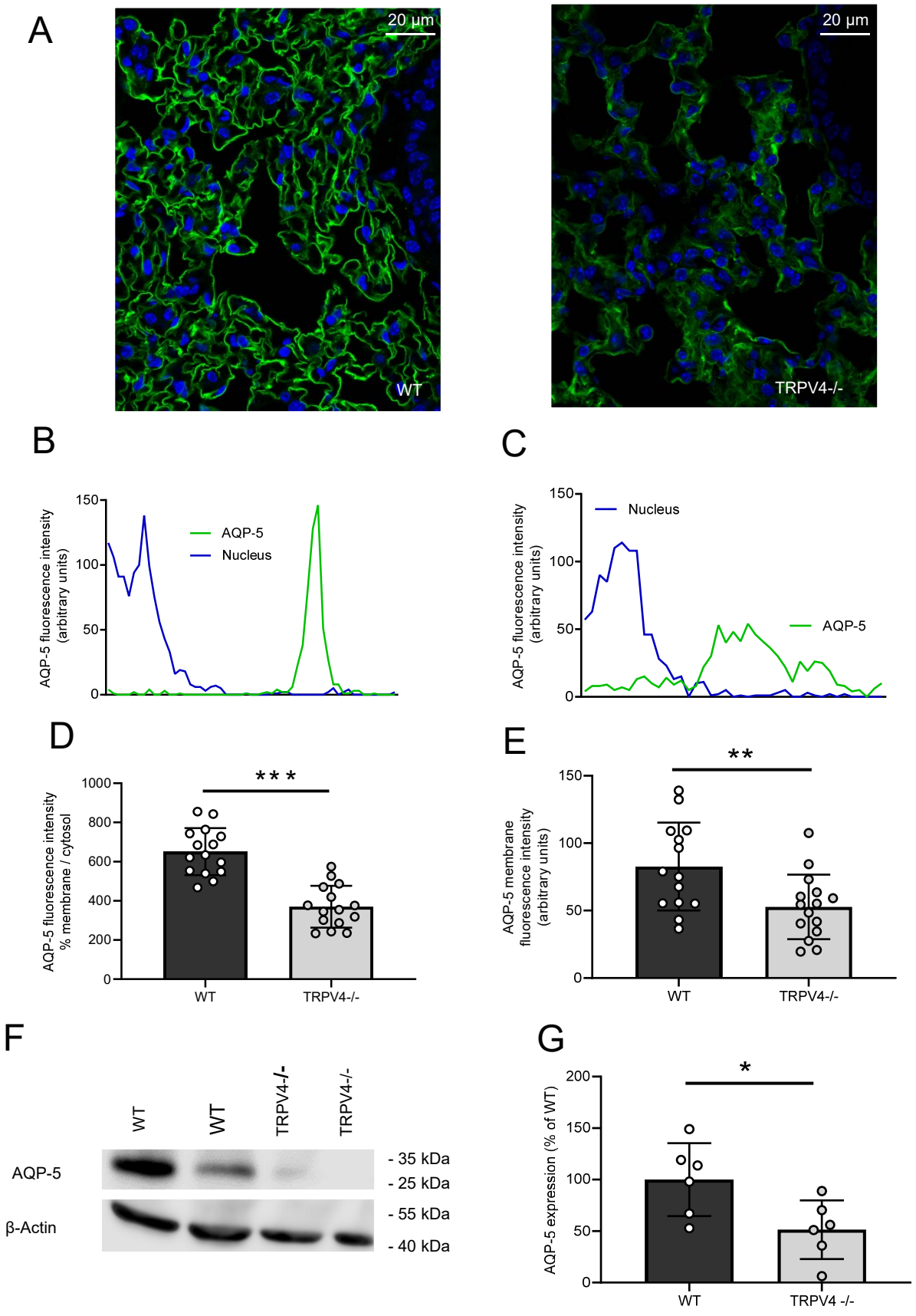
A
20 µm
WT
20 µm
TRPV4-/-
B
AQP-5 fluorescence intensity (arbitrary units)
150
100
50
0
AQP-5
Nucleus
C
AQP-5 fluorescence intensity (arbitrary units)
150
100
50
0
Nucleus
AQP-5
D
AQP-5 fluorescence intensity % membrane / cytosol
1000
800
600
400
200
0
***
WT
TRPV4-/-
E
AQP-5 membrane fluorescence intensity (arbitrary units)
150
100
50
0
**
WT
TRPV4-/-
F
WT
WT
TRPV4-/-
TRPV4-/-
AQP-5
β-Actin
- 35 kDa
- 25 kDa
- 55 kDa
- 40 kDa
G
AQP-5 expression (% of WT)
200
150
100
50
0
*
WT
TRPV4 -/-

Figure 3

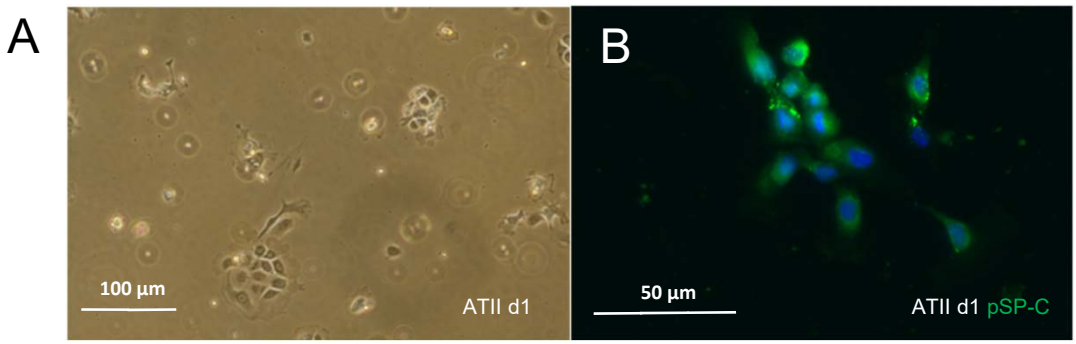
A
100 µm
ATII d1
B
50 µm
ATII d1 pSP-C

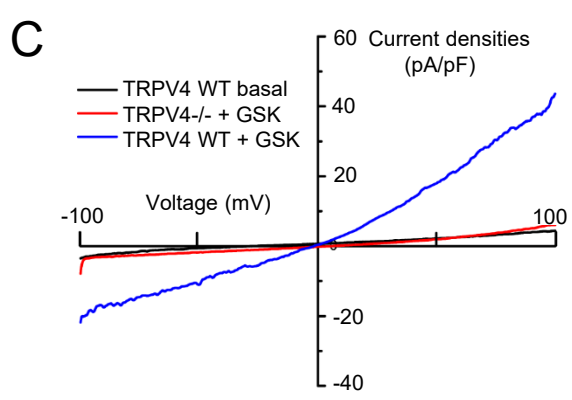
C
60 Current densities (pA/pF)
TRPV4 WT basal
TRPV4-/- + GSK
TRPV4 WT + GSK
40
20
Voltage (mV)
-100
100
-20
-40

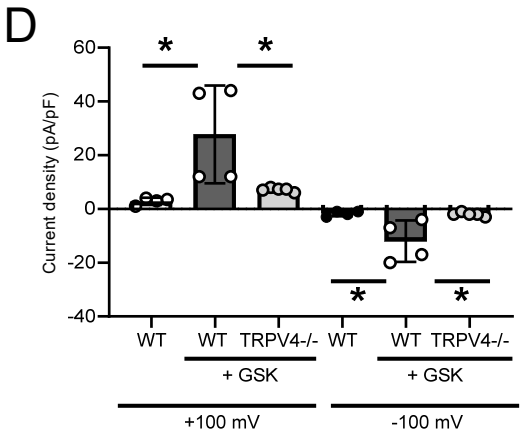
D
*
*
60
40
20
0
-20
-40
Current density (pA/pF)
WT
WT
TRPV4-/-
WT
WT
TRPV4-/-
+ GSK
+ GSK
+100 mV
-100 mV

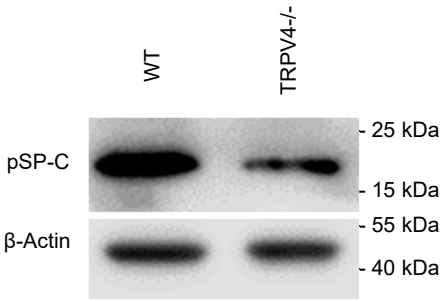
E
WT
TRPV4-/-
pSP-C
β-Actin
25 kDa
15 kDa
55 kDa
40 kDa

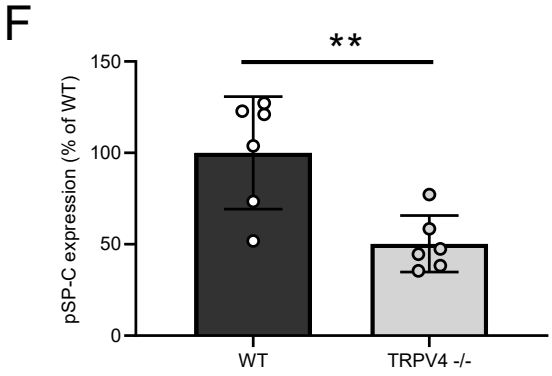
F
**
150
100
50
0
pSP-C expression (% of WT)
WT
TRPV4 -/-

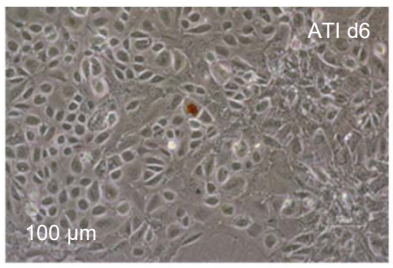
G
ATI d6
100 µm

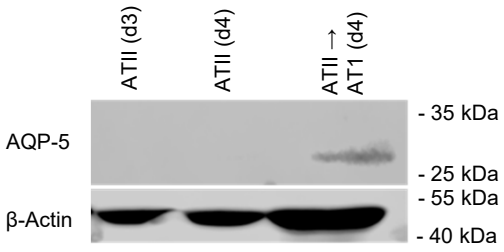
H
ATII (d3)
ATII (d4)
ATII → AT1 (d4)
AQP-5
β-Actin
35 kDa
25 kDa
55 kDa
40 kDa

Figure 4

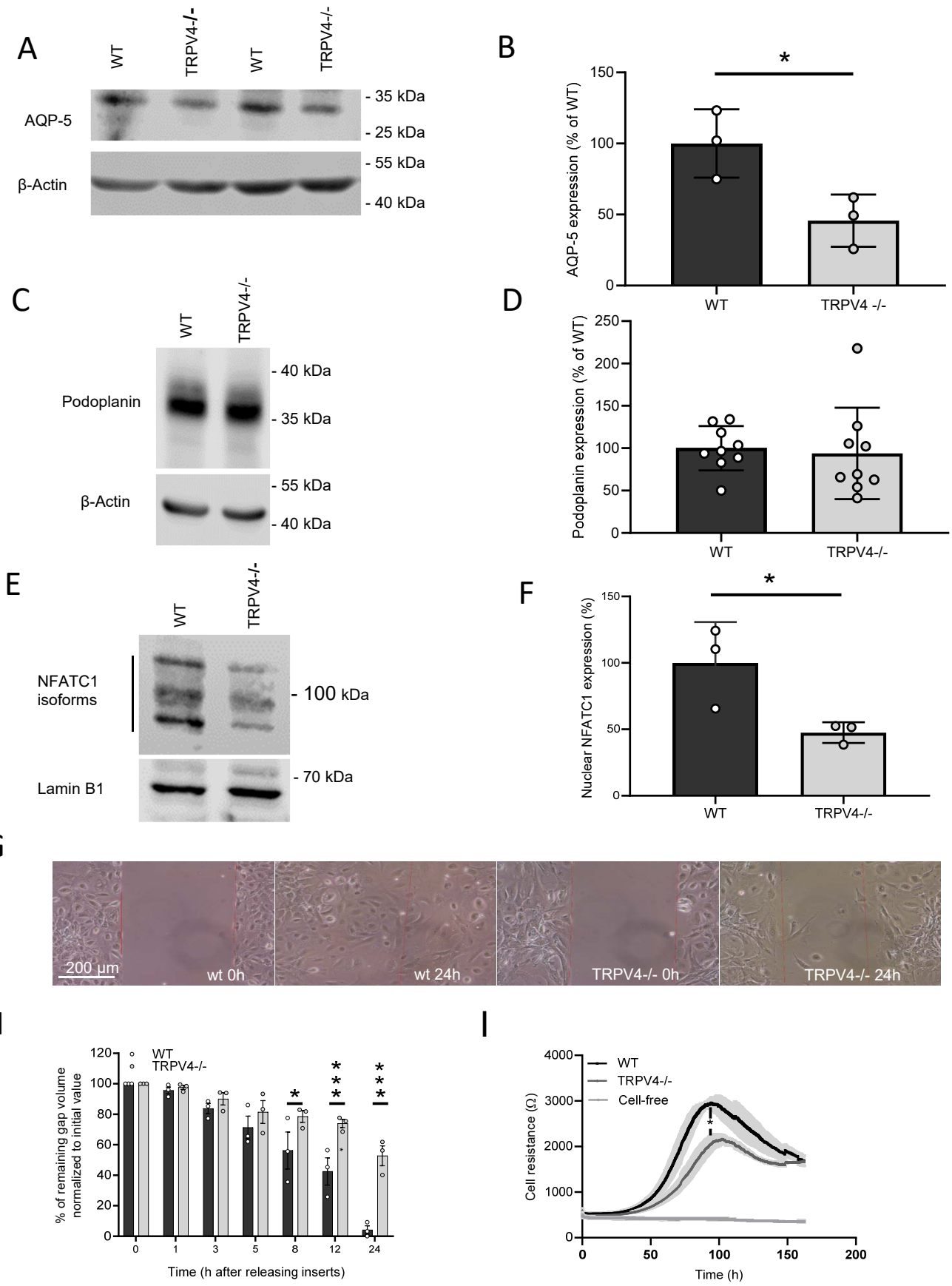
A
WT
TRPV4-/-
WT
TRPV4-/-
AQP-5
β-Actin
- 35 kDa
- 25 kDa
- 55 kDa
- 40 kDa
B
AQP-5 expression (% of WT)
150
100
50
0
*
WT
TRPV4 -/-
C
WT
TRPV4-/-
Podoplanin
β-Actin
- 40 kDa
- 35 kDa
- 55 kDa
- 40 kDa
D
Podoplanin expression (% of WT)
250
200
150
100
50
0
WT
TRPV4-/-
E
WT
TRPV4-/-
NFATC1 isoforms
Lamin B1
- 100 kDa
- 70 kDa
F
Nuclear NFATC1 expression (%)
150
100
50
0
*
WT
TRPV4-/-
G
200 µm
wt 0h
wt 24h
TRPV4-/- 0h
TRPV4-/- 24h
H
% of remaining gap volume normalized to initial value
120
100
80
60
40
20
0
WT
TRPV4-/-
*
*
*
*
*
0
1
3
5
8
12
24
Time (h after releasing inserts)
I
Cell resistance (Ω)
4000
3000
2000
1000
0
WT
TRPV4-/-
Cell-free
*
0
50
100
150
200
Time (h)

Figure 5

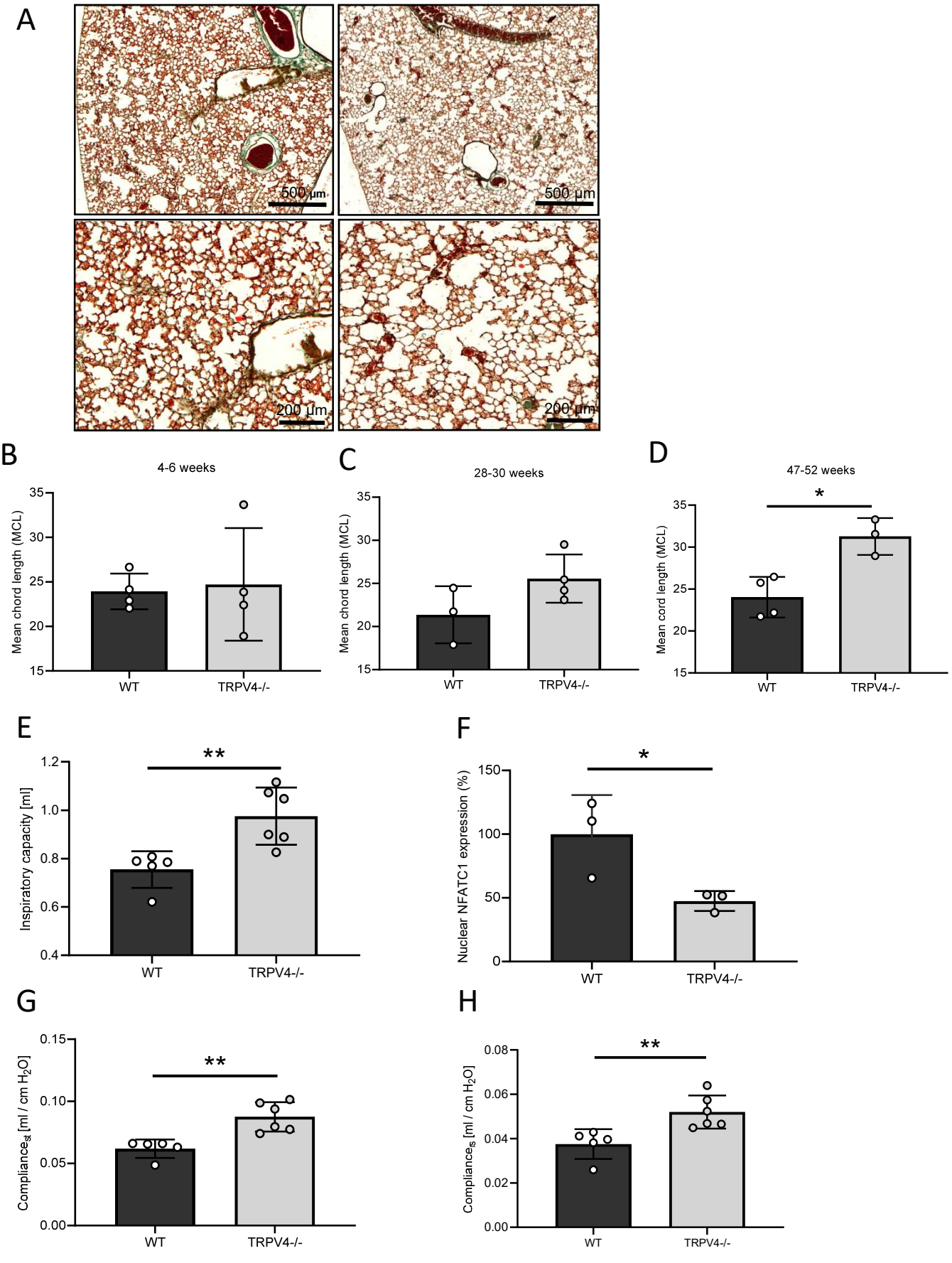
A
500 µm
500 µm
200 µm
200 µm
B
4-6 weeks
Mean chord length (MCL)
WT
TRPV4-/-
C
28-30 weeks
Mean chord length (MCL)
WT
TRPV4-/-
D
47-52 weeks
*
Mean cord length (MCL)
WT
TRPV4-/-
E
**
Inspiratory capacity [ml]
WT
TRPV4-/-
F
*
Nuclear NFATC1 expression (%)
WT
TRPV4-/-
G
**
Compliance$_{st}$ [ml / cm H$_2$O]
WT
TRPV4-/-
H
**
Compliance$_{ts}$ [ml / cm H$_2$O]
WT
TRPV4-/-

Figure 6